Rev. Mexicana Astron. Astrof., **22**, 197-212 (1991)

THE NUCLEAR RING OF THE BARRED GALAXY NGC 1326[1,2]

J.A. García-Barreto[3,4], R.-J. Dettmar[5], F. Combes[6,7]
M. Gerin[6,7], and B. Koribalski[4]

Received 1990 October 31

RESUMEN

Se han realizado observaciones de la emisión de radio continuo, de Hα, de CO(1 − 0) y (2 − 1) y del cercano infrarojo (*J*, *H* y *K*) de la galaxia espiral con barra NGC 1326. El principal resultado de nuestras observaciones es la detección de una estructura circunnuclear tanto en radio continuo como en Hα que corresponde a lo que se conoce como un anillo nuclear. Las observaciones de radio continuo y de Hα indican la existencia de una alta formación estelar que da lugar a la emisión de radiación térmica a través de regiones H II y la emisión de radiación tipo sincrotrón a través de la subsecuente evolución de las estrellas masivas en supernovas y remanentes de supernovas.

ABSTRACT

We have carried out observations of the radio continuum, Hα, CO(1 − 0) and CO(2 −1) and near infrared (*J*, *H* and *K*) emission from the early-type barred spiral galaxy NGC 1326. Our main result is that we have detected in the radio continuum and in Hα a circumnuclear structure that would correspond to a so-called nuclear ring at a mean distance of about 300 pc from the nucleus. The mean radio continuum spectral index, using the integrated total fluxes is $\alpha = -0.7$ ($S_\nu \propto \nu^\alpha$), but it is flatter when using the fluxes of individual sources suggesting a superposition of thermal and non-thermal radiation. The radio continuum and Hα emissions indicate an enhanced star formation activity in the ring giving rise to the thermal emission from H II regions and the non-thermal emission from the evolution of massive stars into supernovae and supernova remnants. Our CO observations indicate a global ratio R(2 − 1)/R(1 − 0) of ∼1.6±0.1 suggesting that part of the emission is from optically thin, warm and dense gas. This warm and dense gas must be associated with intense star formation and this strongly suggests that the CO emission comes essentially from the Hα ring. Our CO angular resolution is not sufficient to resolve the molecular gas structure but the observed spectra show two main spectral components at velocities similar to the observed velocities in Hα from the nuclear ring, supporting the Hα-CO association. We observe optical line ratios Hα/[N II] ∼1.78 and Hα/[S II] ∼3.80 from the nuclear ring indicating radiative ionization and radiative plus collisional excitation mechanisms similar to those in circumnuclear H II regions. We interpret the presence of the two rings (nuclear and outer ring) as due to the gravitational perturbation of the bar. Their common orientation (PA 90°) supports this interpretation where both rings and the bar are in the same plane, in contrast to the polar ring hypothesis (Mebold *et al.* 1979). By combining our near infrared photometry with previously published values with a 5.5" aperture the central mass inside 180 pc is estimated to be 1.6×10^9 $M_\odot$.

Key words: **GALAXIES-BARRED – INFRARED PHOTOMETRY – RADIO-CONTINUUM – STARS-FORMATION**

1. Partly based on observations obtained at ESO, La Silla (Chile).
2. Partly based on observations collected at the Observatorio Astronómico of San Pedro Mártir, B.C., México.
3. Instituto de Astronomía, Universidad Nacional Autónoma de México.
4. Max-Planck-Institut für Radioastronomie, Germany.
5. Radioastronomisches Institut der Universität, Bonn, Germany.
6. DEMIRM, Observatoire de Meudon, France.
7. Radioastronomie Millimetrique, ENS, France.

I. INTRODUCTION

Hawarden *et al.* (1986) have shown from a statistical analysis of IRAS measurements of normal spiral galaxies that barred spiral galaxies have enhanced 25 μm fluxes and they interpret this as arising in regions of active star formation within 20 arcsec of the galactic nuclei. Numerical simulations have predicted the formation of ring structures in galaxies at the locations of resonances, in particular at the Inner and Outer Lindblad Resonances (Schwartz 1981, 1984; Combes and Gerin 1985; Combes 1988).

Buta (1986a) identifies rings in galaxies, in order of increasing relative sizes, as: *nuclear rings* when the structures are found in the center of the galaxy; *inner rings* when the structure are observed around the bars of barred spiral galaxies, and *outer rings* when the structures are found enveloping the main bodies of lenticulars or early spirals. Nuclear rings would then indicate an enhancement of the local density at a distance of a few hundred parsecs from the nucleus. There are two limitations in order to detect nuclear rings: one is that in general barred spiral galaxies are weak radio emitters and the second is that high resolution observations are needed.

In order to select candidates to map their radio continuum emission, we have used the following criteria: they should be barred spirals; their IRAS colors R(60/100) = log [$f_\nu(60)/f_\nu(100)$] and R(12/25) = log [$f_\nu(12)/f_\nu(25)$] should be indicative of enhanced star formation activity after Helou (1986) who has shown that galaxies spread out along a band of progressively greater star formation activity such that the smaller their flux ratio between 12 and 25 μm R(12/25), the larger their ratio between 60 and 100 μ R(60/100); their derived dust temperature from IRAS assuming $S_\nu \sim \nu B_\nu(T)$ should be in the range from 25 to 40 K and should have somewhat redder near infrared colors, compared with the colors of normal spiral galaxies. The near infrared colors were determined from our new broad-band near infrared *J*, *H* and *K* photometry observations of the nuclei of barred spiral galaxies from the Shapley Ames Catalog (García-Barreto, Carrasco and Cruz-González 1987).

Thus we have selected the galaxies NGC 1022, NGC 1326 and NGC 4314 in order to map their radio continuum emission. Our observations of NGC 1022 and NGC 4314 are reported elsewhere (García-Barreto *et al.* 1991a,b). The IRAS colors of NGC 1326 are R(60/100) = −0.23 and R(12/25) = −0.46 [as a comparison M82, a starburst galaxy, has R(60/100) = +0.01 and R(12/25) = −0.71 while M33 with a lower star formation rate has R(60/100) = −0.38 and R(12/25) = +0.12]; its dust temperature is 37 K and its near infrared colors are $J - H = 0.73$, $H - K = 0.34$.

NGC 1326 is an early-type barred spiral galaxy classified as RSBa (Sandage and Tammann 1987)

TABLE 1

OBSERVATIONAL PARAMETERS OF NGC 1326

Radio continuum:				
Frequency (GHz)	1.4	1.4	4.8	14.9
VLA array	D	A/B	B/C	C/D
Date of observation	Sep. 1988	Feb. 1989	May 1989	Oct. 1989
Amplitude calibrator	3C48	3C48	3C48	3C48
Flux amplitude calibrator (Jy)	15.76	15.76	5.57	3.45
Bandwidth (MHz)	50	100	100	100
Phase calibrator	0332-403	0332-403	0332-403	0332-403
r.m.s. (mJy/beam)	1.5	0.07	0.07	0.2
HPBW (arcsec)	90×30	2.9×2.4	3.4×2.6	2.8×2.3
CO:				
Transition	1-0		2-1	
Frequency (GHz)	115.271		230.538	
HPBW (arcsec)	44		22	
Heliocentric velocity (km s^{-1})	1360		1360	
Peak temperature T_{mb} (mK)	~25		~55	
Half power linewidth (km s^{-1})	250		250	
Center of CO map (1950.0)	$\alpha = 03^h22^m01.2^s$, $\delta = -36^\circ38'26''$			

with a lens of about 78" × 60" at P. A. 30° and an outer stellar ring of about 168" × 110" at a P. A. 90°. It is a member of the Fornax I cluster of galaxies, for which we adopt a distance of 13.4 Mpc (Fisher and Tully 1981; Sandage 1978) for H = 100 km s^{-1} kpc^{-1}. Its radio continnuum emission at 5 GHz was first detected as a point source by Whiteoak (1970) with the Parkes 210-ft radio telescope. The full width at half maximum of the beam was 4 arcmin and the position uncertainty was 30" in each coordinate. More recently Condon (1987) has detected its radio continuum emission at 1.49 GHz using the *VLA* in its most compact configuration with a beam of about 60". Mebold *et al.* (1979) observed atomic hydrogen, H I, with the Parkes 210-ft telescope and suggested that the emission is predominantly associated with the outer ring. Wiklind and Henkel (1989) have observed CO(1 − 0) from the central region of NGC 1326 with a HPBW of 44" of the SEST telescope. In addition, Devereux (1987) has successfully detected 10 μm emission from the central region of NGC 1326.

In this paper, we present new high resolution observations of the radio continuum emission from the central region of the barred spiral galaxy NGC 1326 at 1.49, 4.86 and 14.9 GHz, of the optical R band continuum and Hα emission, of the CO(1 − 0) and CO(2 − 1) emission and near infrared broadband photometry at λ1.25, 1.65 and 2.2 μm, with a 14" aperture.

II. RADIO CONTINUUM OBSERVATIONS

The observations were made with the *VLA*[8]. The observational parameters are given in Table 1. The data were edited and calibrated using the on-site *VLA* programs as described by Thompson *et al.* (1980). The data from both circular polarizations in two passbands of 50 MHz bandwidth each centered on 1.465 and 1.515 GHz were combined to produce 1.49 GHz total intensity maps; those at 4.835 and 4.885 GHz were combined to produce 4.86 GHz total intensity maps and those at 14.915 and 14.965 GHz were combined to produce 14.94 GHz total intensity maps. The resulting maps were then "cleaned" (Clark 1980). The low resolution observation at 1.49 GHz in the D-array was used to obtain the total flux and to determine any extended structure. The synthesized beamwidths and r.m.s. noises of the high resolution maps are also listed in Table 1. In order to compute the spectral index from the observed sources we produced additional maps at all observed frequencies with identical HPBWs of 3.6" × 3". The r.m.s. noises observed were similar as those reported before. No attempt was made to measure the linearly polarized emission because it would have required longer integration times in order to obtain a good signal to noise ratio.

8. The *VLA* is a facility of the National Radio Astronomy Observatory and is operated by Associated Universities under contract with U.S. National Science Foundation.

TABLE 2

BACKGROUND SOURCES IN THE FIELD OF NGC 1326 AT 1.49 GHZ

R.A. (1950.0)	Dec. (1950.0)	Peak Flux Density[a] (mJy)
$03^h21^m28.4^s$	−36°30' 26.8"	18
03 21 40.6	−36 40 31.6	81
03 21 57.6	−36 46 09.5	10
03 22 10.7	−36 42 19.5	27
03 22 34.3	−36 39 46.1	12
03 22 39.0	−36 45 54.6	20
03 23 03.1	−36 53 50.6	12

a. No attempt has been made to correct for primary beam dilution. Beam FWHM ~ 90" × 30".

III. RADIO CONTINUUM RESULTS

a) *Low Resolution Map*

Our primary motivation to carry out a low resolution observation of NGC 1326 was to determine whether there was any radio emission from the outer stellar ring or whether the radio emission was concentrated to the central region as reported previously by Whiteoak (1970) and Condon (1987). Our low resolution (θ_{HPBW} ~ 90" × 30") observation at 1.4 GHz showed the emission as originating from an unresolved source with a peak flux S_ν ~ 31±1 mJy/beam. This flux is in agreement with a flux of 35 mJy reported by Whiteoak (1970) and a flux of 29.4 mJy reported by Condon (1987). No radio continuum extended emission (> 30") was detected to a level of 1.5 mJy/beam at 1.4 GHz and no radio continuum emission was detected from the outer stellar ring. A list of positions and fluxes of background sources at 1.49 GHz is given in Table 2.

b) *High Resolution Radio Continuum Maps of the Central Region*

Our high resolution (θ_{HPBW} ~ 3") observations, however, resolve the central emission into several sources around the compact nucleus. The full resolution maps at each frequency are shown in

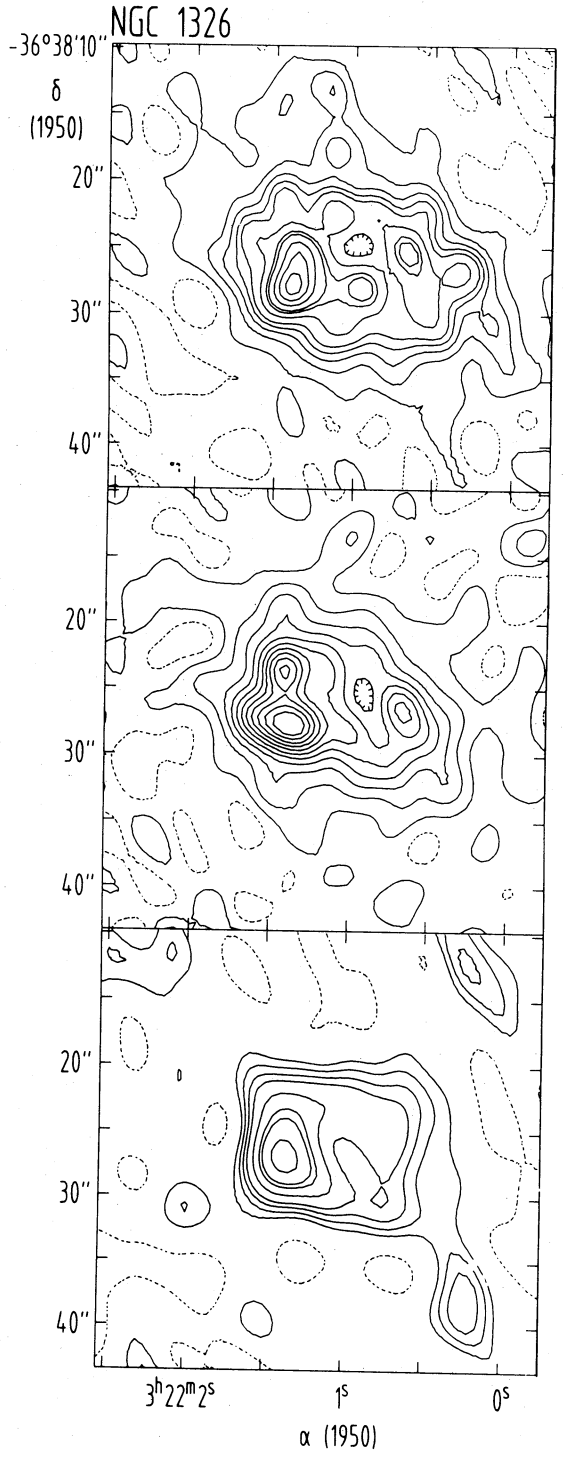

Fig. 1. High resolution maps of the radio continuum emission from NGC 1326 at 20 (top), 6 (middle) and 2 cm (bottom). The contour levels on all maps are −1, 1, 3, 5, 7, 11, 13, 15, 19, 24, 29, 34, 39, 44 in units of 0.066 mJy/beam area except in the 2 cm map where the first contours are −3 and 3 in the same units. Restoring beams are 2.9" × 2.5", 3.4" × 2.6" and 5" × 3.6"at 20, 6 and 2 cm, respectively.

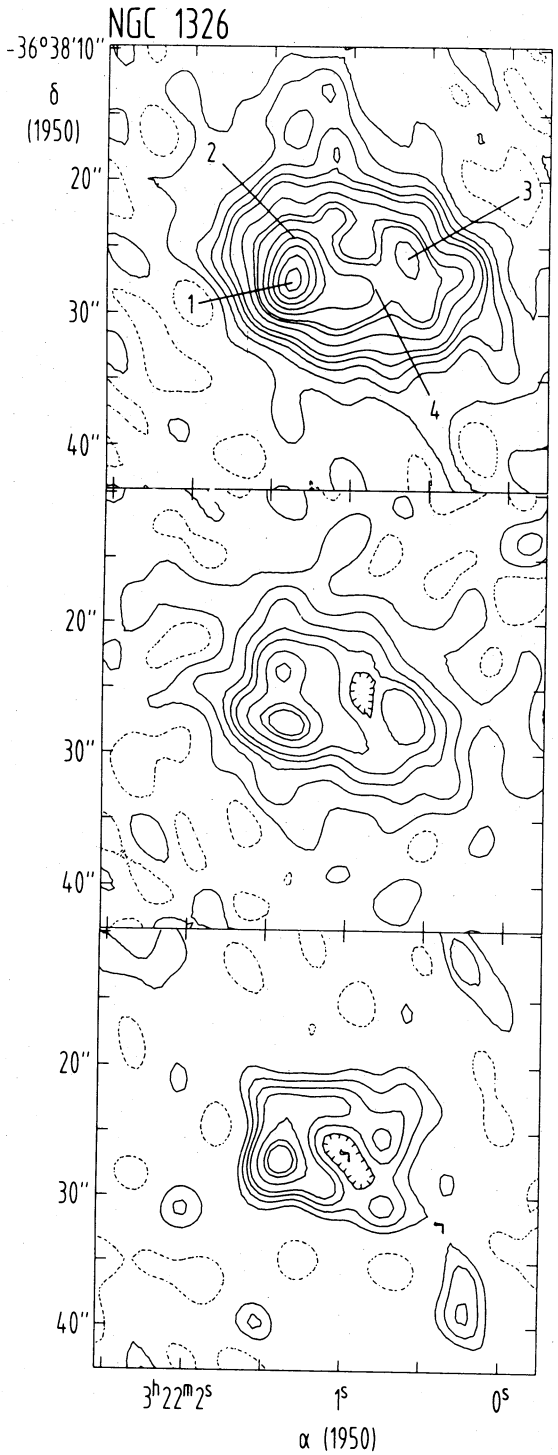

Fig. 2. High resolution maps of the radio continuum emission from NGC 1326 at 20 (top), 6 (middle) and 2 cm (bottom) with the same restoring beam of 3.6" × 3". The contour levels in all three maps are the same as in Figure 1.

Figure 1. In Figure 2 we present again the maps at the three frequencies but with a similar restoring clean beam of 3.6" × 3". The high resolution observations are not sensitive for the larger (> 30") scale structure and thus the flux densities obtained correspond to the inner 30" region. We obtained integrated fluxes of 25±0.5 mJy at 1.49 GHz, 11.1±0.3 mJy at 4.86 GHz and about 5±1 mJy at 14.94 GHz. The corresponding spectral indices, using the integrated flux at all observed frequencies are similar, $\alpha = -0.7$ ($S_\nu \propto \nu^\alpha$). This spectral index is similar to that determined toward the radio ring structure in two other galaxies, namely NGC 1097 (Hummel, van der Hulst and Keel 1987a) and NGC 4314 (García-Barreto *et al.* 1991b) using integrated fluxes. With this spectral index and the total flux at 20 cm from our low resolution map we can estimate the total flux at 6 cm and at 2 cm. The estimated total fluxes are 14±1 mJy at 6 cm and 6±1 mJy at 2 cm. The radio continuum emission from NGC 1326 has been clearly resolved into several sources less than 5" in diameter at the three frequencies embedded in a diffuse emission. We interpret the radio continuum emission as arising from a ring structure around the position of the compact nucleus with an inner radius of 3", an outer radius of about 6" and a mean radius, given by the ridge of radio emission, of about 4.5", i.e., 300 pc at an assumed distance of 13.4 Mpc. This structure would correspond to a nuclear ring according to the terminology of Buta (1986a). Similar radio continuum nuclear rings have been observed in NGC 613 (Hummel *et al.* 1987b), NGC 1097 and NGC 4314 (García-Barreto *et al.* 1991b). In NGC 613 and NGC 1097 there is a strong radio continuum emission clearly associated with the compact nucleus. In NGC 1326 there is no strong radio emission clearly associated with the compact nucleus to a limit of 1.5 mJy/beam at 20 cm. As can be seen in Figure 3 the radio continuum emission in NGC 1326 is clearly dominated by the nuclear ring. Comparable circumnuclear structures within a radius of less than 1.5 kpc have been detected in the optical from several spiral and barred spiral galaxies (Arsenault *et al.* 1988; Kennicutt, Keel and Blaha 1989). Positions 1, 2 and 3 shown in Figure 2 indicate three unresolved sources in the nuclear ring where we have determined their flux densities at 1.49, 4.86 and 14.94 GHz. Position 4 indicates a local minimum in the flux at the three frequencies with a flux at 14.94 GHz of about 0.29 mJy/beam or 1σ, suggesting that most of the emission is then of non-thermal origin. Figure 4 shows the radio continuum spectra for the integrated fluxes and for the peak fluxes for source 1, while Figure 5 (Plate) shows the radio continuum emission superimposed on a POSS optical photograph.

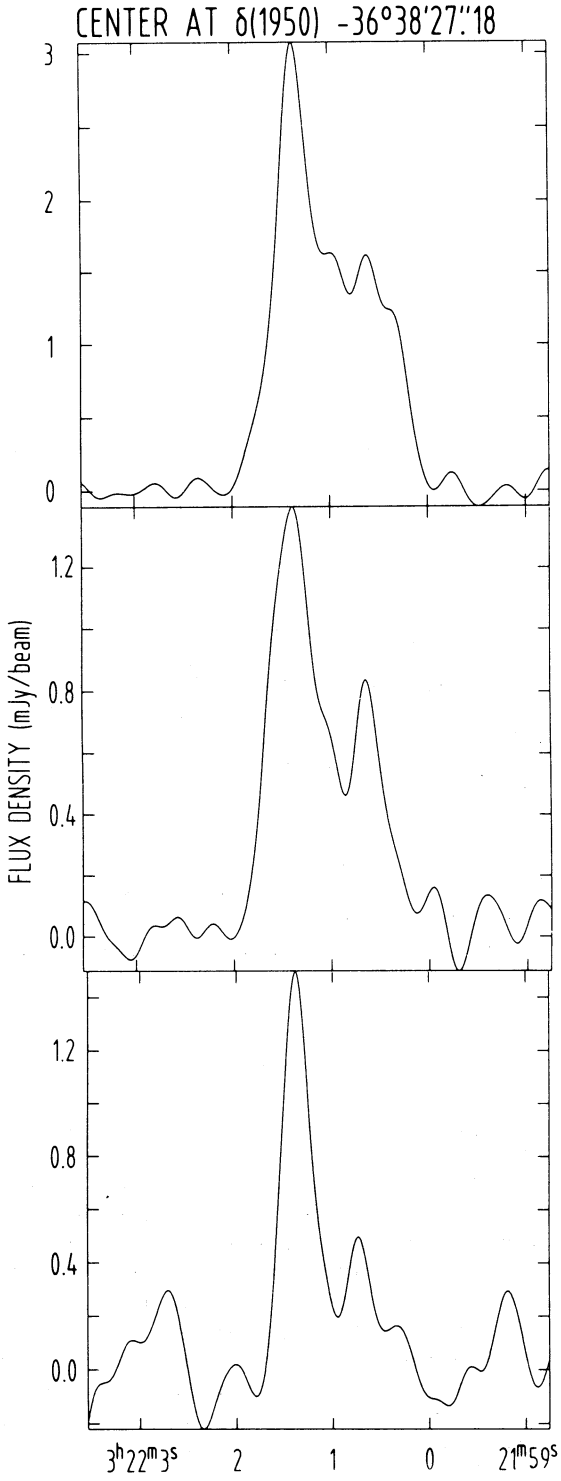

Fig. 3. East-west brightness distributions at 20 (top), 6 (middle) and 2 cm (bottom) from the maps in Figure 2 along declination $\delta = -36°38'27.18"$. Notice that the emission is dominated by the ring.

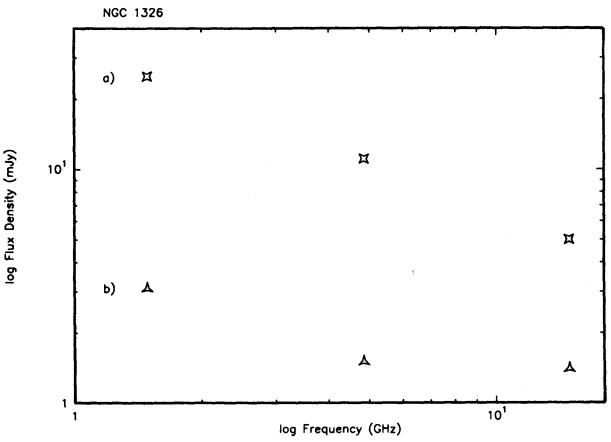

Fig. 4. Radio continuum spectra of the central region of NGC 1326. a) (upper): integrated flux. b) (lower): peak flux from source 1 as shown in Figure 2.

c) *Separation of Thermal and Non-Thermal Radio Emission*

In general we can assume that the total observed radio continuum emission at each frequency from spiral galaxies is the sum of two terms, namely, a term involving optically thin synchrotron radio continuum emission from relativistic particles interacting with the ambient magnetic field, $S_{NTH} \propto \nu^{-\alpha}$, where α is the synchrotron spectral index, and a term involving optically thin free-free radio continuum emission from H II regions, $S_{TH} \propto \nu^{-0.1}$. Thus at each frequency, ν, the observed flux density is

$$S_T = A_1\nu^{-\alpha} + A_2\nu^{-0.1} \quad , \qquad (1)$$

where A_1 and A_2 are frequency independent factors. To solve simultaneously for A_1, A_2 and α is not simple because equation (1) is not a linear equation. Our main interest is to determine the thermal emission from the unresolved sources found in the nuclear ring of NGC 1326. For this purpose we can use our observations of the flux at the three frequencies 1.49, 4.86, and 14.94 GHz done with identical angular resolution. An expression for the thermal flux at 14.94 GHz (2 cm) in terms of the observed fluxes at 1.49 and 4.86 GHz and in terms of α would be (see Appendix for details):

$$S_2^{TH} = \frac{S_{20}^T\left(\frac{\nu_2}{\nu_{20}}\right)^{-0.1} - S_6^T\left(\frac{\nu_{20}}{\nu_6}\right)^{-\alpha}\left(\frac{\nu_2}{\nu_{20}}\right)^{-0.1}}{\left[1-\left(\frac{\nu_{20}}{\nu_6}\right)^{-\alpha}\left(\frac{\nu_6}{\nu_{20}}\right)^{-0.1}\right]} \quad , \qquad (2)$$

where S_2^{TH} is the thermal flux at 14.94 GHz (2 cm), and S_{20}^T and S_6^T are the observed total flux at 1.49 and 4.86 GHz (20 and 6 cm), ν_{20}, ν_6 and ν_2 are the frequencies 1.49, 4.86 and 14.94 GHz respectively and α is the non-thermal spectral index. One way to estimate α would be to find a source with no thermal emission, such that the observed fluxes at two frequencies would be all due to synchrotron emission. One would then assume that the value of α found at that location would be the same characteristic value of the synchrotron emission at other places. In the case of NGC 1326 we have followed that method and estimated the spectral index α from a place with a minimum flux at 14.94 GHz. This place is shown in Figure 2 as position 4. The estimated spectral index was $\alpha = -0.85$. We then assumed that this spectral index was characteristic of the spectral index value of the underlying diffuse emission in the ring structure, and estimated the thermal fluxes from sources labeled 1, 2 and 3 in Figure 2.

We have checked that this value of α is reasonable for the underlying diffuse emission in the ring of NGC 1326 by the following method. We estimated the fluxes from the underlying diffuse emission at each frequency by subtracting the sum of the fluxes of the 3 unresolved sources shown in Figure 2 from the total integrated fluxes of the ring structure. We then assumed that all of these fluxes were of non-thermal origin and estimated α using two observations at a time as shown in case 2 in the Appendix. The observed values were between $\alpha = -0.78$ and $\alpha = -1.1$. We obtain that at least 40% of the emission from source number 1 is thermal emission at 6 cm while about 80% is thermal emission from source number 2.

Assuming a thermal flux at 6 cm of source number 1 $S_\nu \sim 0.6$ mJy/beam, a source size of about 4", an electron temperature of 10^4 K and spherical geometry, we may compute the characteristic electron density using the relation by Mezger and Henderson (1967)

$$\frac{N_e}{cm^3} = 7.233\times10^3\left(\frac{T_e}{10^4\ K}\right)^{0.175}\left(\frac{\nu}{GHz}\right)^{0.05} \times \times\left(\frac{S_\nu}{mJy}\right)^{0.5}\left(\frac{D}{kpc}\right)^{-0.5}\left(\frac{\theta_G}{arcsec}\right)^{-1.5} \quad . \qquad (3)$$

We then find $N_e \geq 8$ cm^{-3}, an emission measure, EM = 2.5×10^4 pc cm^{-6}, and ionized gas mass of $M_i = 5 \times 10^6$ $M_\odot$. The corresponding number of Lyman continuum photons is estimated to be $N_{Lyc} \simeq 9.5 \times 10^{51}$ s^{-1} (Scoville *et al.* 1983) which would correspond to at least 2×10^3 O7 zero age main sequence stars (Panagia 1973).

From the thermal flux, the expected Hα flux, F, is (Lequeux 1980):

$$\frac{F(H\alpha)}{erg\ cm^{-2}\ s^{-1}} = 8.75 \times 10^{-13} \left[\frac{S_\nu}{mJy}\right] \times \times \left[\frac{\nu}{GHz}\right]^{0.1} \left[\frac{T_e}{10^4\ K}\right]^{-0.34} \quad (4)$$

For S_{TH} = 0.6 mJy/beam at 6 cm we obtain F(Hα) ≃ 6.1 × 10^{-13} erg cm^{-2} s^{-1} for an individual region, and for a sum of at least three main radio sources as seen in Figure 2, the expected Hα flux is F(Hα) ≃ 1.8 × 10^{-12} erg cm^{-2} s^{-1}.

IV. Hα OBSERVATIONS AND RESULTS

CCD images were obtained in November 1990 with the ESO 2.2-m telescope on La Silla (Chile). We used a GEC chip with 22 μm pixel which results in a field of view of 1.7' × 2.5' covering only the central bar of the galaxy. Continuum images were obtained in the Thuan and Gunn *r*-filter with exposure times of 5 min and 10 min. An image of 40 min exposure time was taken through a filter with Δλ(FWHM) = 76.9 A centered on λ_c = 6596.9 A and including the redshifted emission lines of Hα and [N II].

After standard reduction for bias subtraction, flat fielding with dome flats, and cosmic ray filtering the frames were aligned and the overexposed central part of the 10 min *r*-band image was replaced by the scaled short exposure image. The sky level for all images was determined in the SE corner of the field just outside of the outer ring. The probable error of the sky determination due to the small field does not influence the results for the bright central parts discussed in the following.

The combined, sky-corrected *r*-band image was finally scaled to the exposure level of the continuum in those parts of the image obtained in the Hα filter that are emission-line free as judged from an iterative procedure. Absolute photometry of this *r*-band image was performed by simulated aperture photometry for the five measurements given by de Vaucouleurs and Longo (1988) with aperture < 100". The actual count rate combined with the equivalent width of the Hα filter and the absolute calibration by Tüg, White and Lockwood (1977) result in a flux determination for the *r*-band continuum and the continuum-corrected Hα image.

In addition, a long-slit spectrum was obtained at the 1.52-m ESO telescope with the B&C spectrograph, again using a GEC CCD chip. The wavelength range between λ6200 A and λ7000 A was covered with a dispersion of 1.4 A/pixel. The slit was oriented in E-W direction, centered on the nucleus.

In Figures 6a and 6b (Plate) we present the continuum frames in a grey-scale and contour representation, the latter converted to *R*-band magnitudes. The bar at position angle PA = 35° is clearly visible, it ends at a distance r ≃ 37" (or 2.4 kpc) from the nucleus. Parts of the outer ring are visible in the NE and SW corners. The nuclear region shows asymmetries and a non-regular increase in surface brightness caused by the Hα emitting ring. A dust lane is crossing the SW part of the bar at r ≃ 20" from the nucleus.

Figure 7 gives the continuum-corrected Hα emission. The Hα/[N II] line ratio derived from our spectrum was used to correct for the contribution of [N II] within the filter. Most of the emission originates in a ring-like structure which shows individual knots. The mean radius of these knots is r ≃ 5".2. Weaker line emission is associated with the nucleus and we notice a number of very faint emission regions along the direction of the bar.

The total integrated flux of the central 20" in Hα is F(Hα) = 1.38 × 10^{-12} erg cm^{-2} s^{-1}. This is in very good agreement with the thermal flux as derived in §III and reassures us that the assumptions made there are reasonable. The ratio of the meas-

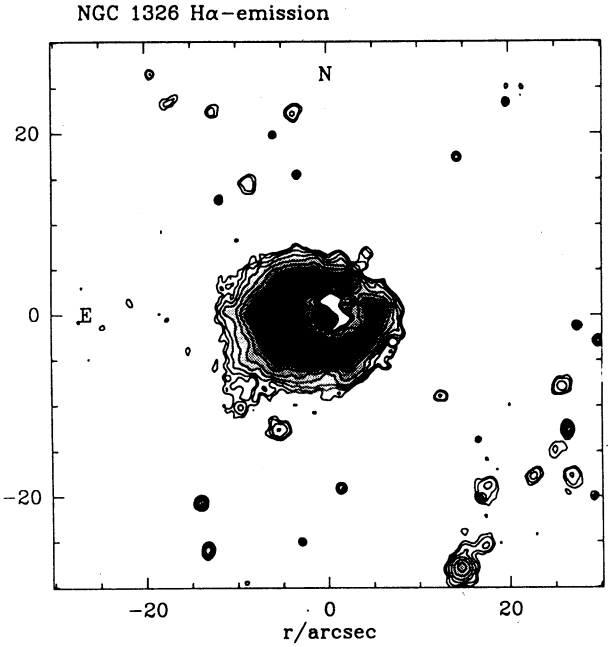

Fig. 7. Grey and contour image of the continuum-free line emission Hα+[N II] of the central region of NGC 1326 taken at ESO 2.2-m telescope on La Silla (Chile). The lowest contour is 0.5 × 10^{-16} erg cm^{-2} s^{-1} $arcsec^{-2}$ and subsequent contours increase by a factor of 2. The flux calibration for the Hα contours was estimated using the Hα/[N II] line ratio.

ured Hα flux to the expected flux derived from the thermal continuum would correspond to a dust absorption of $A_{H\alpha} \simeq 0.3$ mag.

In Figure 8 we give the spectra of the eastern and western regions of the ring as observed by the slit. The measured line parameters from Gaussian fits to the emission and the radial velocities are summarized in Table 3. From the [S II]λλ6718/6731 ratio we estimate an electron density of $n_e \simeq 100$ cm^{-3} (Osterbrock 1989).

V. MILLIMETRIC OBSERVATIONS AND RESULTS

The millimetric observations were made in November 1989 with the 15-m Swedish-ESO telescope (SEST) in La Silla (Chile). The half-power beamwidth is ~ 44" at $^{12}CO(1-0)$ (115 GHz) and ~ 22" at $^{12}CO(2-1)$ (230 GHz).

We used Schottky mixers with SSB receiver temperatures of 300 K and 700 K for the 115 and 230 GHz lines respectively. The system temperature and the antenna temperature corrected for telescope and atmospheric losses were established by means of chopper wheel calibrations. The total system temperature outside the atmosphere was T_{sys} = 450 K and 1100 K for the 115 and 230 GHz lines respectively. We adopt in this paper the main beam temperature scale (T_{mb}), quite fitted for the small size of the source (Kutner and Ulich 1981). The main beam efficiencies used to obtain T_{mb} are, for the 115 and 230 GHz lines, 0.68 and 0.51, respectively.

The backend was an acousto-optical spectrometer with 728 channels each 690 KHz wide. The data were smoothed to a velocity resolution of 14.6 km s^{-1}. All velocities quoted here are heliocentric.

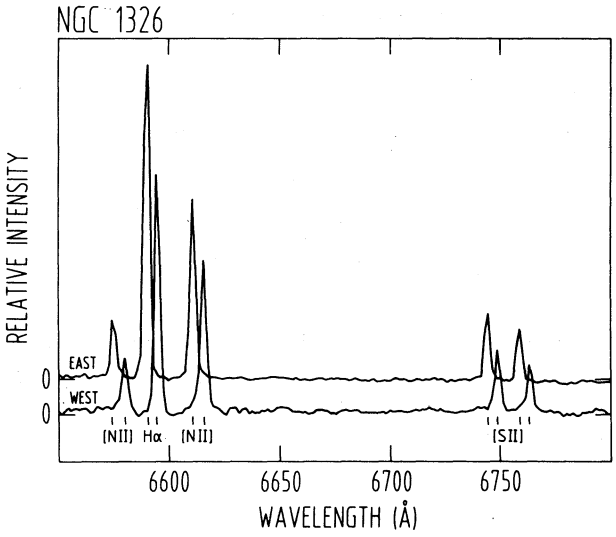

Fig. 8. Optical emission lines from the eastern (top) and western (bottom) part of the central Hα emission from NGC 1326 at a PA 90°. The long-slit spectrum was obtained at the 1.52-m ESO telescope on La Silla (Chile).

We used a 6 Hz dual beam-switching procedure with two symmetric reference positions offset by 12' in azimuth. We integrated typically one hour on each point. Pointing was checked at least every two hours by observations of radio sources, planets and SiO masers. The r.m.s. pointing errors were about 5". The observational CO parameters are displayed in Table 1.

The CO spectra are displayed in Figure 9. The source is barely resolved in the $CO(2-1)$ line by the 22" beam, the extension of the source is of the order

TABLE 3

OPTICAL EMISSION LINES IN THE NUCLEAR RING OF NGC 1326

Line	Rest Wavelenght	Eastern Region					Western Region				
	(A)	λ (A)	V^a (km s^{-1})	I_{Rel}[e]	FWHM[b] (A)	FWHM[a] (km s^{-1})	λ (A)	V^a (km s^{-1})	I_{Rel}[e]	FWHM[b] (A)	FWHM[a] (km s^{-1})
Hα	6562.8	6590.0	1243[c]	2129	1.05	48[d]	6595.0	1471[c]	914	1.05	48[d]
[N II]	6548.1	6575.2	1241	344	1.28	58	6580.1	1465	175	1.66	76
[N II]	6583.4	6610.8	1248	1192	1.28	58	6615.7	1471	574	1.98	90
[S II]	6716.4	6744.5	1254	383	1.47	65	6749.3	1469	199	1.98	88
[S II]	6730.8	6759.0	1256	279	1.82	81	6763.9	1474	142	1.82	81

a. Velocities computed from $V = ((\lambda_{obs} - \lambda_{ref})\, c/\, \lambda_{ref})$, where c is the velocity of light. b. Deconvolved line width with an instrumental FWHM ~2.38 A. c. A typical error in the velocity determination is ±5 km s^{-1}. d. A typical error in the velocity width is ±3 km s^{-1}. e. Relative intensity.

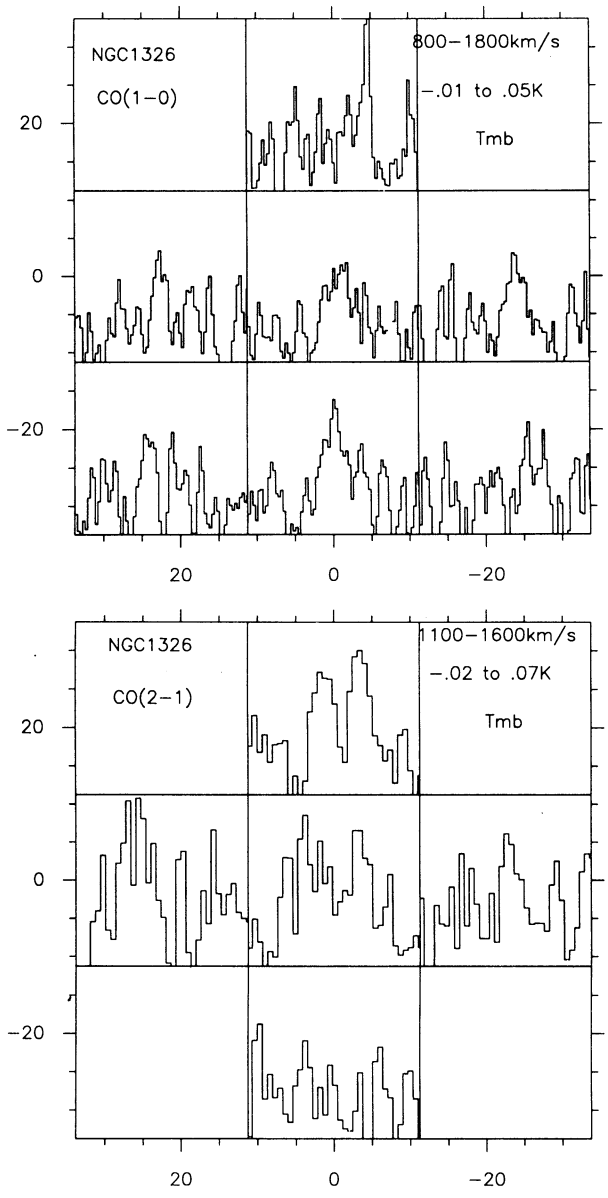

Fig. 9. a) CO(1 − 0) and b) CO(2 − 1) spectra obtained towards NGC 1326 with the SEST 15-m telescope. The velocity resolution is degraded to 14.6 km s^{-1}. The spatial resolutions are 44" and 22" respectively.

of 24" = 1.6 kpc. The CO(2 − 1) spectra reveal two velocity components, which could correspond to a molecular ring in rotation, or be the consequence of a highly rising rotation curve. At an offset 22" east, we see only the low-velocity component, while at an offset 22" west, we only see the high-velocity one. This is compatible with a rotating disk with a position angle of 90°, similar to the optical PA of the outer stellar ring. The two components are separated by 200 km s^{-1}, while the width of the average spectrum is $\Delta V \sim 250$ km s^{-1} at half power. This gives an order of magnitude of maximum rotation velocity: 230 km s^{-1} in the plane of the galaxy if the inclination of 50° is adopted (Mebold et al. 1979).

The total mass of molecular hydrogen observed is $M(H_2) \sim 2.2 \times 10^8\ M_\odot$, with an adopted $N(H_2)/I(CO)$ conversion ratio of 2.3×10^{20} H_2 molecules cm^{-2}/K km s^{-1}. This compatible, within the error bars, with the value quoted by Wiklind and Henkel (1989), when scaled to the same distance, and to the same H_2/CO conversion ratio. The maximum H_2 surface density is of the order of 1.4×10^{21} H_2 cm^{-2}, which is a lower limit to the true maximum, when dilution is taken into account. The estimated H_2 mass to CO luminosity is $M(H_2)/L_{CO} \simeq 3.6$.

To get some insight in the CO line excitation, we have convolved the CO(2 − 1) map to the 44" resolution. Figure 10 displays the superposition of the CO(1 − 0) and (2 − 1) spectra. The global ratio in integrated intensity is R(2 − 1)/R(1 − 0) = 1.6±0.1. Certainly, to ensure that this ratio is correct, it is better to map the whole galaxy in both transitions CO(1 − 0) and CO(2 − 1) but our observations seem to indicate that there is CO only in the center. This ratio, larger than 1, could mean that a significant fraction of the emission comes from an optically thin, hot and dense gas in the center. The average ratio in normal spiral galaxies is near 0.5 (Braine *et al.* 1991), which would suggest

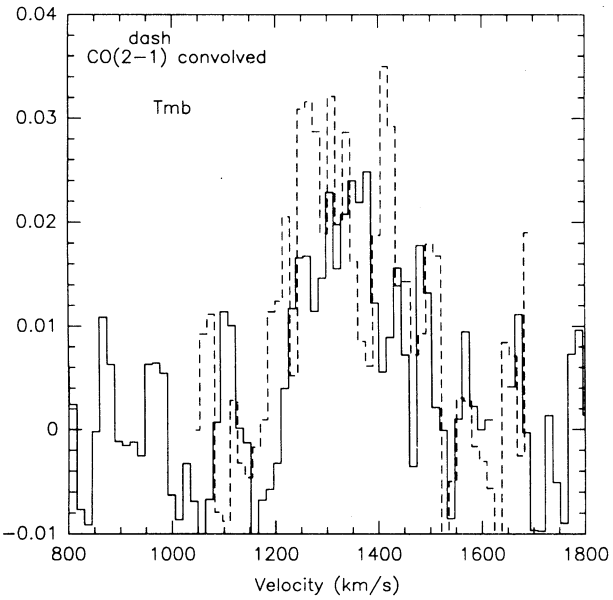

Fig. 10. Superposition of the convolved CO(2 − 1) spectrum with the CO(1 − 0) in the center, in the T_{mb} scale. The global ratio of integrated intensity R(2 − 1)/R(1 − 0) is 1.6.

subthermal excitation for the CO(2 – 1) line. Only in some starburst galaxies, where the active region is resolved by the beam, this ratio is observed above 1 (cf., M82, Loiseau *et al.* 1990). The observed ratio of 1.6 in NGC 1326 which refers to a region of 44" (3 kpc in diameter) means that most of the emission comes from a much smaller region, warm and dense, diluted in the beam which is likely in view of the starburst activity indicated by our radio continuum and Hα observations of the nuclear ring. However, as mentioned by Young and Scoville (1984) a second interpretation would be that the clouds could be heated by an external radiation field, rather than by internal sources, raising the temperature on the outside by each cloud.

VI. NEAR INFRARED OBSERVATIONS AND RESULTS

The near infrared observations were made with the 2.12-m telescope in San Pedro Mártir, Baja California, México in 1987 September 10. We used a single element InSb detector at J (1.25 μm), H (1.65 μm) and K (2.2 μm) bands at the f/31 Cassegrain focus (Roth *et al.* 1984). The beam size was 14" and the 10 Hz chopper throw was 100" in declination. The photometry was calibrated on SAO stars (Tapia, Neri and Roth 1986). Several 5-sec scans were taken at each wavelength at the position of the H-band peak. Flux densities were computed relative to a scale of 1520, 980 and 620 Jy at 1.25, 1.65 and 2.2 μm respectively for a zero-mag star (Beckwith *et al.* 1976). Table 4 lists our 2.2 μm measurements with a 14" aperture and those of Devereux *et al.* (1987) with a 5.5" aperture. Our photometry uncertainty is about 0.02 mag at 2.2 μm or about 10 mJy. Assuming that the 2.2 μm growth curve can be described by a single power law (Devereux 1989) and that the flux dependence on aperture size is represented as a power law of index γ, then combining our 2.2 μm measurements, with a 14" aperture, with those of Devereux *et al.* (1987), with a 5.5" aperture, we obtain $\gamma = 1.22$ for NGC 1326. Devereux *et al.* (1987) have estimated the mass in the inner region of galaxies using nuclear velocity dispersion and multi-aperture 2.2 μm observations. In principle then, if we knew the nuclear velocity dispersion in NGC 1326, we could use our 2.2 μm measurements to estimate the mass in the inner region ($r < 450$ pc). However, because we lack nuclear velocity dispersion measurements for NGC 1326, no good estimate of the central mass can be given. We can however use our Hα velocity determinations from the eastern and western regions of the nuclear ring. The observed velocities are ~ 115 km s^{-1} blue and redshifted from the systemic velocity respectively when taking $V_{sys} \simeq 1362$ km s^{-1} (Fisher and Tully 1981; Tully 1988).

Following Devereux *et al.* (1987) the central mass is

$$M(r) = 233\ \beta\ r_{pc}\ \sigma^2_{km\ s^{-1}}\ M_\odot\ ,$$

where σ is the nuclear velocity dispersion, the mass density distribution ρ(r) is expressed as a power law of the form $\rho(r) \propto r^{-\beta}$, and β is determined from multiaperture 2.2 μm measurements under the assumption that the mass and luminosity share the same radial dependence. Taking σ as the mean observed Hα velocity corrected for an inclination of 50°, $\sigma \simeq 150$ km s^{-1}, and β as 1.78, we then obtain $M(< 180\ pc) \simeq 1.6 \times 10^9\ M_\odot$.

TABLE 4

NEAR IR PHOTOMETRY OF THE CENTRAL REGION OF NGC 1326

Filter Band	λ (μm)	Flux Density 5.5"[a] Aperture (mJy)	14" (mJy)
J	1.25	60	188±10
H	1.65	79	236±10
K	2.2	64	201±10
N	10.2	105±42	...

a. Fluxes in 5.5" aperture from Devereux *et al.* (1987).

VII. DISCUSSION

a) *Geometry of the Nuclear Ring*

The most interesting feature of the radio continuum and Hα emissions from NGC 1326 is the ring structure in the central region ($r < 1$ kpc). Similar nuclear radio ring structures have been observed towards other barred spiral galaxies as NGC 613 (Hummel *et al.* 1987b), NGC 1097 (Hummel *et al.* 1987a) and NGC 4314 (García-Barreto *et al.* 1991b). In NGC 1326, as in NGC 4314, the radio continuum emission is dominated by the nuclear ring and not by a radio source that could be associated with the compact nucleus. The observed structure in NGC 1326 is not circular but elliptical with a major axis orientation at PA 90°. The major axis orientation agrees with the major axis of the outer stellar ring but the present observations do not give as good estimates for the orientation of the extended radio continuum diffuse emission. From the lower contours of the maps there is a slight indication that the extended difusse emission is indeed along a PA 30° similar to the lens (Fig. 5).

b) *Star Formation in the Nuclear Ring*

By mapping the radio continuum emission at three frequencies (1.49, 4.86 and 14.94 GHz) one can separate the thermal and non-thermal emission components. It has been shown that at least 40% of the radio continuum emission from NGC 1326 is thermal emission. This corresponds to a thermal total emission from the central region at 6 cm of $S_{TH} \simeq 5$ mJy. The observed line ratios are Hα/[N II] $\simeq$ 1.78 and Hα/[S II] $\simeq$ 3.80. In order to determine whether the observed ratios in NGC 1326 are similar to normal disk H II regions or to circumnuclear H II regions it is necessary to have other diagnostic line ratios as Hβ/[O III] or [O II]/[O III] (Kennicutt *et al.* 1989). Unfortunately we do not have these additional ratios for NGC 1326. Our probable detection of weak [O I]λ6300 in the eastern part of the ring gives a ratio Hα/[O I] $\sim$ 35 which is similar to normal H II regions. Our Hα/[N II] ratio, however, suggests that the [N II] emission is somewhat strong and as discussed by Kennicutt *et al.* (1989) it could arise from either high nitrogen abundant regions or from shock-heated gas. Although high heavy-element abundances could produce strong forbidden-line emission, most metal-rich disk H II regions show weak forbidden line emission (Kennicutt *et al.* 1989). Thus the observed Hα/[N II] and Hα/[S II] ratios in the nuclear ring of NGC 1326 seem to be more similar to circumnuclear H II regions where the main ionization mechanism is photoionization from massive stars and the somewhat strong [N II] and [S II] emissions could indicate regions where the gas is additionally shock-excited. These arguments strongly indicate the presence of massive luminous stars, that is, enhanced star formation in the nuclear ring. The additional mechanism could likely be the excitation mechanism in the ring of NGC 1326 as suggested by the CO line ratios, and the rate of supernovae and supernova remnants from the natural evolution of the stars that are being formed in the nuclear ring. From the radio thermal emission and Hα from the nuclear ring 10 μm emission would be expected to be associated with this structure. Following Genzel *et al.* (1982), the expected central 10 μm emission would be $S_{10\mu m} \simeq 20\ S_{TH}$, i.e., in NGC 1326 $S_{10\mu m} \simeq 100$ mJy. In their model Genzel *et al.* (1982) assumed that the 10 μm radiation is emitted by hot grains inside H II regions being heated by Lyα photons; the grains emitting in the 60 to 100 μm far-IR, with temperature less than 40 K, are probably located outside the H II regions where they absorb luminosity at a rate equal to that of all the OB stars. Since 10 μm emission has been detected with a flux of $S_{10\mu m} \simeq 105 \pm 42$ mJy from the nuclear region with an aperture of 5.5" (Devereux 19987), the expected additional 10 μm emission distribution would be similar to the Hα and radio continuum emission distribution. Similar distribution of the emissions of Hα, 10 μm and radio continuum has been observed towards the barred galaxy NGC 1097 (Telesco and Gatley 1981; Hummel *et al.* 1987a). Recent IUE observations of NGC 1326 also suggest that the *UV* flux originates from an ensemble of young stars (Danks, Pérez and Altner 1990). A star formation rate of OBA stars can be estimated using SFR $\sim 8 \times 10^{-11}\ L_{TOT}\ M_\odot\ yr^{-1}$ (Scoville and Young 1983). For NGC 1326 the far-infrared luminosity derived from IRAS flux measurements is $L_{FIR} = 2.4 \times 10^9\ L_\odot$ while its blue luminosity is $L_B = 9.3 \times 10^9\ L_\odot$ (Fisher and Tully 1981). With $L_{TOT} = L_{FIR} + L_B$ we have for NGC 1326 $L_{TOT} = 1.2 \times 10^{10}\ L_\odot$ and the corresponding global star formation rate is SFR $\simeq 0.96\ M_\odot\ yr^{-1}$, that is about 10 times higher than the mean SFR found in Virgo spiral galaxies (Scoville *et al.* 1983). From our Hα observations the star formation rate in the nuclear ring using SFR $\sim 0.89 \times 10^{-41}\ L(H\alpha)\ M_\odot\ yr^{-1}$ (Kennicutt 1983) is SFR $\sim 0.22\ M_\odot\ yr^{-1}$. Although similar values are observed from early-type spiral galaxies (Kennicutt 1983) using the integrated Hα disk emission, the star formation rate found in NGC 1326 refers only to the nuclear ring and suggests an enhancement of star formation in the central 600 pc.

Assuming that this star formation rate is uniform over the ring, of inner radius 3" and outer radius 6" inclined 50° to the line of sight, then the star formation rate per unit is $0.6\ M_\odot\ yr^{-1}\ kpc^{-2}$ which is about 10 times the global rate in our Galaxy of 5 $M_\odot\ yr^{-1}/\pi\ (5\ kpc)^2$ or $0.06\ M_\odot\ yr^{-1}\ kpc^{-2}$ (Güsten and Mezger 1983).

c) *Gas Content of the Nuclear Ring*

How much gas is there in NGC 1326? From our single dish CO observations we determine a molecular hydrogen mass of $2.2 \times 10^8\ M_\odot$ at a distance of 13.4 Mpc, in agreement with the estimated value of Winklind and Henkel (1989). Our observations are not suitable to say if the gas is in a ring structure that could be associated with the nuclear ring. From the CO(2 – 1) velocity profile it is found that the spectrum is dominated by two peaks separated by approximately 200 km s^{-1}. This velocity width agrees with the velocity difference of the Hα components straddling the nucleus, which is of the order of 230 km s^{-1}. In analogy with other galaxies, as e.g., NGC 1097 (Gerin, Nakai and Combes 1988) and NGC 4314 (García-Barreto *et al.* 1991b) where the molecular gas is clearly associated with the central radio structure, one may assume that this is also the case in NGC 1326. The gas mass ratio $M(H_2)/M(H\ I)$ in NGC 1326 is ≥ 0.07.

TABLE 5

SUMMARY OF DERIVED PARAMETERS FOR NGC 1326

Radio continuum measurements:			
Frequency (GHz)	1.49	4.86	14.94
Total integrated flux (mJy)	31	...	...
	35[a]	...	...
	29[b]	...	...
Central integrated flux (mJy)	25±0.5	11.1±0.3	5±1
Peak flux[c] (mJy/beam)	3.1	1.4	1.4
Radio map mean position (1950.0)	$\alpha = 03^h22^m01^s$, $\delta = -36°38'26''$		
Mass estimates:			
H_2 mass ($M_\odot$)	2.2×10^8		
H I mass[d] ($M_\odot$)	1.7×10^9		
Gravitational mass (r < 180 pc) ($M_\odot$)	1.6×10^9		
H II mass ($M_\odot$)	$< 2\times10^7$		
Resonant model:			
Corotation radius (kpc)	4 ≃ end of the bar		
Inner Lindblad resonance (pc)	200-400		
Angular velocity at ILR (km s^{-1} kpc^{-1})	Ω(300 pc) ≃ 385		
Bar pattern speed (km s^{-1} kpc^{-1})	$\Omega_p = 60$		
Outer Lindblad resonance (kpc)	6		
Star formation in ring:			
R(2 − 1)/R(1 − 0)[e]	1.6		
Hα luminosity (erg s^{-1})	3×10^{40}		
Lyman continuum photons[c] (s^{-1})	9×10^{51}		
Star formation rate[f] ($M_\odot$ yr^{-1})	0.22		
Star formation rate/kpc^2 ($M_\odot$ yr^{-1} kpc^{-2})	0.6		
Global parameters:			
FIR luminosity[g] ($L_\odot$)	2.4×10^9		
Blue luminosity[h] ($L_\odot$)	9.3×10^9		
Global star formation rate[i] ($M_\odot$ yr^{-1})	0.96		
Distance adopted[h] (Mpc)	13.4		
Inclination[j]	50°		
Position angle of bar[j]	30°		
Position angle of nuclear ring	90°		
Position angle of outer ring	90°		
cz[h] (km s^{-1})	1362		
Dust temperature[k] (K)	37		
Ratios:			
$L_{FIR}/M(H_2)$	11		
$M(H_2)/M_G$	0.1		
$M(H_2)/M_T$	0.003		
$M(H_2)$/Area nuclear ring ($M_\odot$ pc^{-2})	580		

a. Total flux from single dish observation (Whiteoak 1970). b. Total flux from *VLA* ($\theta \sim 60''$) observation (Condon 19987). c. From source 1 shown in Figure 2. Beam FWHM ~ 3"×3". d. Total H I measurements (Mebold *et al.* 1979). The H I is however believed to be associated with the outer stellar ring. e. Ratio of the integrated intensity after convolving the CO(2 − 1) map to 44" resolution. f. Star formation rate from Hα luminosity of ring using SFR ~ 0.89×10^{-41} L(Hα) $M_\odot$ yr^{-1} (Kennicutt 1983). g. From IRAS fluxes at $L_{FIR} \simeq 4\pi D^2$ FIR, where FIR = 1.26×10^{-14} (2.58 f_ν(60 μm) + f_ν(100 μm)). h. Fisher and Tully (1981). i. O, B, A star formation rate using SFR ~ 8×10^{-11} L_{TOT} $M_\odot$ yr^{-1} where L_{TOT} is far infrared plus blue luminosities (Young and Scoville 1983). j. Mebold *et al.* (1979). k. From IRAS 60 μm and 100 μm fluxes assuming $S_\nu \sim \nu B_\nu(T)$.

However high resolution observations of H I are required to give a better estimate for this ratio in the nuclear ring, since most of the H I flux is believed to be associated with the outer stellar ring (Mebold *et al.* 1979). The ratio of gas mass to gravitational mass in the inner region is $M(H_2)/M_G$(r < 450 pc) ≃ 0.1; the ratio of molecular mass to the total mass is $M(H_2)/M_T \simeq 0.003$ ($M_T \simeq 4.0 \times 10^{10}$, Mebold *et al.* 1979) and $L_{FIR}/M(H_2) \sim 10$. In order to produce 30 $M_\odot$ stars at the current rate of star formation the gas reservoir will only last a few times 10^7 years and therefore it may be transitory unless it is replenished continuously. Table 5 summarizes the derived parameters for the nuclear ring of NGC 1326.

d) *Origin of the Nuclear Ring Structure*

The symmetry of the radio continuum and the Hα emissions and the molecular hydrogen concentration observed in the central 30" region of NGC 1326 indicate that the ring structure is a zone of enhanced gas densities compared to surrounding regions. Such zones of enhanced gas densities are most likely related to orbital resonances due to galaxy dynamics.

The existence of these rings depends primarily on the radial dependence of the angular velocity of the gas and stars, Ω(r), the epicyclic frequency (radial oscillation), κ(r), and very important, the angular velocity pattern of the bar, Ω_p [see for example Figure 6 of Combes (1988)]. Nuclear rings are expected to be found at inner Lindblad resonances (ILR) as shown by Schwartz (1981, 1984), Combes and Gerin (1985), Buta (1986a, 1986b, 1987) and Combes (1988). In order to

check the validity of this hypothesis we constructed a mass model for the galaxy, integrating all constraints from the near infrared distributions, and kinematical information from Hα and CO data. The model is based on three components: a bulge represented by a Plummer sphere of characteristic radius 0.6 kpc and mass 1.8×10^{10} $M_\odot$; a Toomre thin disk (1963) of characteristic radius 4.5 kpc and mass 6×10^{10} $M_\odot$; and an extended halo, with 13 kpc scale and mass comprised within the optical disk of 5×10^{10} $M_\odot$. The latter does not modify the central rotation curve, but ensures its flatness at large radii. The rotation curve from this model is displayed in Figure 11 together with the derived angular velocity curve $\Omega(r)$ and $\Omega(r) \pm \kappa(r)/2$.

From these curves, we can determine the position of Lindblad resonances of the bar wave, and check whether the nuclear and outer rings are both produced by the same bar pattern. Let us take for the size of the bar its dimension along the PA = 30° (i.e., 84" in diameter or 5.7 kpc) that we deproject, assuming it belongs to the plane defined by the outer ring, inclined by 50° with PA 90°. The true diameter of the bar would then be 8.2 kpc. If we assume that the bar ends at its corotation (Contopoulos 1980), then the corotation can be chosen at 4 kpc. This value implies an outer Lindblad resonance (OLR) at ~6 kpc (i.e., the radius where $\Omega_p = \Omega(r) + \kappa(r)/2$) and the ILR at ~300 pc (i.e., the radius where $\Omega_p = \Omega(r) - \kappa(r)/2$) both of which correspond roughly to the positions of the rings in NGC 1326. The angular velocity pattern of the bar, Ω_p, would then be $\Omega_p \sim 60$ km s^{-1} kpc^{-1}. The mass model, although not unique, is compatible with the observations and shows that our interpretation is coherent: the rings could have been formed by the same bar pattern, represented by the elongated stellar component at PA 30°.

It is worth noting that NGC 1326 is a member of Fornax I cluster of galaxies, group 51−1 of Tully (1988) that contains about 30 galaxies within 1 Mpc from NGC 1326 and in particular NGC 1326A and NGC 1326B lie within 65 kpc. Therefore an interaction with a neighbour galaxy would be possible, given the short relative distance among them, and perhaps it could have also triggered the central activity in NGC 1326.

VIII. CONCLUSIONS

Our high resolution observations of the radio continuum and Hα emissions from NGC 1326 show a ring structure around the compact optical nucleus. From our CO observations we were able to estimate the molecular mass and the line ratio R(2 − 1)/R(1 − 0). From our optical spectroscopy we were able to compute optical line ratios and estimate the

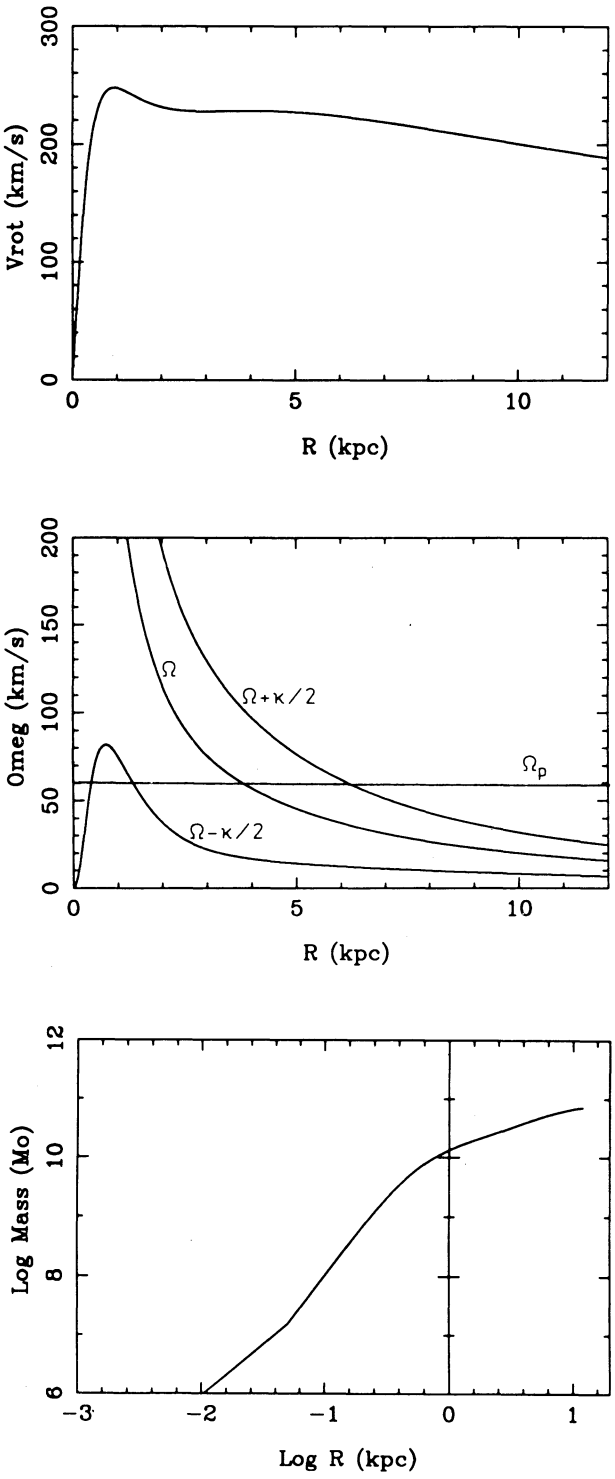

Fig. 11. Mass distribution, angular velocity and rotation curve for NGC 1326 as a function of radius from our model (see text). $\Omega(r)$ represents the angular velocity of gas and stars; $\kappa(r)$ is the epicyclic frequency (radial oscillation) and Ω_p is the angular velocity pattern of the bar. ILR is found at a radius where $\Omega_p = \Omega(r) - \kappa(r)/2$; OLR is found at a radius where $\Omega_p = \Omega(r) + \kappa(r)/2$ (see text).

electron densities. Our infrared observations allow us to give an approximate estimate of the central (r < 450 pc) mass. Specific conclusions are:

1) The radio continuum and central Hα emissions indicate a circumnuclear structure within 300 pc from the nucleus that would correspond to a nuclear ring according to the terminology of Buta (1986a).

2) The radio continuum emission is dominated by the ring emission, and no strong radio source ($S_\nu <$ 1.5 mJy/beam at 1.49 GHz) can be associated with the compact nucleus.

3) Our high resolution observations of the radio continuum at 1.49, 4.86 and 14.94 GHz resolve the emission into several sources that lie embedded in a ring structure of radius r $\simeq$ 4.5", with flat spectral indices ($\alpha > -0.6$). By combining our observations at the three frequencies a thermal emission of at least 40% is observed.

4) No radio continuum emission was detected from extended regions (r > 40") or from the outer stellar ring to a level of 1.5 mJy/beam.

5) The mean spectral index of the total integrated central flux is $\alpha = -0.7$ ($S_\nu \sim \nu^\alpha$). The spectral index of the underlying diffuse emission was estimated as $\alpha \simeq -0.85$.

6) From the estimated radio thermal flux at 6 cm a typical electron density of H II regions of > 8 cm^{-3} is derived. The Lyman continuum photon rate of each radio component is equivalent to about 2×10^3 O7 zero age main sequence stars.

7) From the observed ratio [S II]$\lambda\lambda$6718/6731 from the ring emission an electron density is estimated to be $n_e \leq 100$ cm^{-3}.

8) The observed Hα/[N II] $\sim$ 1.7 and Hα/[S II] $\sim$ 3.8 in the ring of NGC 1326 indicate radiative ionization and radiative plus collisional excitation characteristic of H II regions.

9) The molecular mass in the central 44" of NGC 1326 was estimated as $M(H_2) \sim 2.2 \times 10^8$ M$_\odot$.

10) The CO(1 – 0), CO(2 – 1) line ratio was estimated as R(2 – 1)/R(1 – 0) $\sim$ 1.6 indicating that part of the emission is from optically thin, hot and dense gas.

11) The 2.2 μm flux density varies with radius as $R^{1.22}$ and an approximate estimate of the central mass is derived as $M(< 180$ pc$) \simeq 1.6 \times 10^9$ M$_\odot$.

12) From a mass model which reproduces the observed velocities, an angular velocity pattern of the bar $\Omega_p \sim 60$ km s^{-1} kpc^{-1} would predict an ILR at 300 pc and an OLR at 6 kpc. We thus interpret the presence of the two rings as due to the gravitational perturbation of the bar in contrast to the polar ring hypothesis.

13) From the total (FIR + blue) luminosities, the star formation rate is estimated to be 0.96 M$_\odot$ yr^{-1}, which is about 10 times higher than the average star formation rate in the Virgo spiral galaxies.

The star formation rate in the nuclear ring, from the Hα luminosity, is SFR $\sim$ 0.22 M$_\odot$ yr^{-1}. The star formation rate per unit area is also a factor of 10 higher than the star formation rate in the central 5 kpc in our Galaxy.

The authors would like to thank P. Perley, the staffs of the *VLA* and the Observatorio Astronómico Nacional in San Pedro Mártir, Baja California, México for their help during the observations, G. Breuer for typing the manuscript and G. Hutschenreiter and W. Fusshöller for their photographic work and preparation of the figures. It is a pleasure to thank Dr. M. Dahlem for careful reading of the manuscript. J.A.G-B acknowledges partial financial support by CICB-UAEM (Toluca, México), CONACYT (México) grant PCCBBNA- 022688 and a fellowship from the Alexander von Humboldt-Stiftung, Germany.

REFERENCES

Arsenault, R., Boulesteix, J., Georgelin, Y., and Roy, J.-R. 1988, *Astr. and Ap.*, **200**, 29.
Beckwith, S., Evans, N.J., Becklin, E.E., and Neugebauer, G. 1976, *Ap. J.*, **208**, 390.
Braine, J. *et al.* 1991, in preparation.
Buta, R. 1986a, *Ap. J. Suppl.*, **61**, 609.
Buta, R. 1986b, *Ap. J. Suppl.*, **61**, 631.
Buta, R. 1987, *Bull. A.A.S.*, **19**, 1063.
Clark, B.G. 1980, *Astr. and Ap.*, **89**, 377.
Combes, F. 1988, in *Galactic and Extragalactic Star Formation*, eds. R.E. Pudritz and M. Fich (Dordrecht: Kluwer), p. 475.
Combes, F. and Gerin, M. 1985, *Astr. and Ap.*, **150**, 327.
Condon, J.J. 1987, *Ap. J. Suppl.*, **65**, 485.
Contopoulos, G. 1980, *Astr. and Ap.*, **81**, 198.
Danks, A.C., Pérez, M.R., and Altner, B. 1990,in *Bulges of Galaxies, ESO/CTIO Workshop*, eds. B.J. Jarvis and D.M. Terndrup, ESO Conferences Proceedings No. 35, p. 243.
Devereux, N. 1987, *Ap. J.*, **323**, 91.
Devereux, N. 1989, *Ap. J.*, **346**, 126.
Devereux, N., Becklin, E.E., and Scoville, N. 1987, *Ap. J.*, **312**, 529.
de Vaucouleurs, A. and Longo, G. 1988, *Catalogue of Visual and Infrared Photometry of Galaxies from 0.5 μm to 10 μm (1961-1985)*, University of Texas Monographs in Astronomy No. 5.
Fisher, J.R. and Tully, R.B. 1981, *Ap. J. Suppl.*, **47**, 139.
García-Barreto, J.A., Carrasco, L., and Cruz-González, I. 1987, *Bull. A.A.S.*, **19**, 1033.
García-Barreto, J.A. *et al.* 1991a, *Astr. and Ap.*, in press.
García-Barreto, J.A. *et al.* 1991b, *Astr. and Ap.*, **244**, 257.

Genzel, R. *et al.* 1982, *Ap. J.*, **255**, 527.
Gerin, M., Nakai, N., and Combes, F. 1988, *Astr. and Ap.*, **203**, 44.
Gioia, I.M., Gregorini, L., and Klein, U. 1982, *Astr. and Ap.*, **116**, 164.
Güsten, R. and Mezger, P.G. 1983, *Vistas in Astronomy*, **26**, 59.
Hawarden, T.G., Mountain, C.M., Leggett, S.K., and Puxley, P.J. 1986, *M.N.R.A.S.*, **221**, 41p.
Helou, G. 1986, *Ap. J. (Letters)*, **311**, L33.
Hummel, E., van der Hulst, J.M., and Keel, W.C. 1987a, *Astr. and Ap.*, **172**, 32.
Hummel, E., Jörsäter, S., Lindblad, P.O., and Sandqvist, A. 1987b, *Astr. and Ap.*, **172**, 51.
Kennicutt, R.C. 1983, *Ap. J.*, **272**, 54.
Kennicutt, R.C., Keel, W.C., and Blaha, C.A. 1989, *A.J.*, **97**, 1022.
Kutner, M.L. and Ulich, B.L. 1981, *Ap. J.*, **250**, 341.
Lequeux, J. 1980, in *Star Formation*, eds. A. Maeder and L. Martinet (Gineva Obs.: Switzerland), p. 75.
Loiseau, N. *et al.* 1990, *Astr. and Ap.*, **228**, 331.
Mebold, U., Goss, W.M., van Woerden, H., Hawarden, T.G., and Siegman, B. 1979, *Astr. and Ap.*, **74**, 100.
Mezger, P.G. and Henderson, A.P. 1967, *Ap. J.*, **147**, 471.
Osterbrock, D.E. 1989, *Astrophysics of Gaseous Nubulae and Active Galactic Nuclei* (Mill Valley, CA.: University Science Books), p. 134.
Panagia, N. 1973, *A.J.*, **78**, 929.
Roth, M., Iriarte, A., Tapia, M., and Reséndiz, G. 1984, *Rev. Mexicana Astron. Astrof.*, **9**, 25.
Sandage, A. 1978, *A.J.*, **83**, 904.
Sandage, A. and Tammann, G.A. 1987, *A Revised Shapley-Ames Catalogue of Bright Galaxies*, (Washington, D.C.: Carnegie Institution).
Schwartz, M.P. 1981, *Ap. J.*, **247**, 77.
Schwartz, M.P. 1984, *M.N.R.A.S.*, **209**, 93.
Scoville, N.Z. and Young, J.S. 1983, *Ap. J.*, **265**, 148.
Scoville, N.Z., Becklin, E.E., Young, J., and Capps, R.W. 1983, *Ap. J.*, **271**, 512.
Tapia, M., Neri, L., and Roth, M. 1986, *Rev. Mexicana Astron. Astrof.*, **13**, 115.
Telesco, C.M. and Gatley, I. 1981, *Ap. J. (Letters)*, **247**, L11.
Thompson, A.R., Clark, B.G., Wade, C.M., and Napier, P.J. 1980, *Ap. J. Suppl.*, **44**, 151.
Toomre, A. 1963, *Ap. J.*, **138**, 385.
Tüg, H., White, N.M., and Lockwood, G.W. 1977, *Astr. and Ap.*, **61**, 679.
Tully, R.B. 1988, *Nearby Galaxies Catalog*, (Cambridge: University Press), p. 201.
Whiteoak, J.B. 1970, *Astr. Letters*, **5**, 29.
Wiklind, T. and Henkel, C. 1989, *Astr. and Ap.*, **225**, 1.
Young, J.S. and Scoville, N.Z. 1984, *Ap. J.*, **287**, 153.

APPENDIX

a) *Separation of Thermal and Non-Thermal Radio Continuum Emission*

Our high resolution observations of the radio continuum from barred spiral galaxies with a beam $\theta_{FWHM} \sim 3 - 4$" indicate that the central emission at least from NGC 1326 and NGC 4314 is dominated by a nuclear ring-like structure. This nuclear ring has several unresolved sources on top of a more diffuse emission. The angular resolution translates into a linear dimension of between 150 → 200 pc. The radio continuum radiation from these sources could be of three types.

Case 1: Thermal Emission. The radio continuum emission could be totally due to H II regions. The observed flux density would be assumed to originate from optically thin H II regions,

$$S_\nu^T \sim T_e^{-0.35} \nu^{-0.1} \int_0^L N_e N_i \, dl \quad , \qquad \text{(A.1)}$$

where T_e is the electron temperature, N_e is the electron density, N_i is the proton density and L is the path length that depending on the geometry would be proportional to the angular resolution of the beam. Mezger and Henderson (1967) have shown how to estimate the different parameters from such observations.

Case 2: Synchrotron Emission. The radio continuum emission could be totally of non-thermal origin. Then for an optically thin synchrotron emission

$$S_\nu^T \sim N_0 \, (B \sin\theta)^{\alpha+1} \, L \, \nu^{-\alpha} \quad , \qquad \text{(A.2)}$$

where N_0 is the relativistic particle density, B is the magnetic field strength, θ is the angle the magnetic field makes with the line of sight, L is the path length, and α is the so-called non-thermal spectral index. In order to determine α, then two measurements are needed at two different frequencies with similar angular resolutions. Thus

$$\alpha = [log \, (S_1/S_2)]/[log \, (\nu_2/\nu_1)] \quad . \qquad \text{(A.3)}$$

Case 3: Synchrotron and Thermal Emission. In this case the observed flux density would be the sum of synchrotron emission due to the interaction of relativistic particles with the ambient magnetic field and thermal emission from H II regions. Thus

$$S_\nu^T = C_1\, N_0 (B\, sin\theta)^{\alpha+1}\, L\, \nu^{-\alpha} + \\ + C_2\, T_e^{-0.35} \int_0^L N_e\, N_i\, dl\, \nu^{-0.1} \quad , \qquad \text{(A.4)}$$

where C_1 and C_2 are constants. Writing C_3 and C_4 as constants involving frequency independent factors, then at a given frequency ν, the observed flux density is

$$S_\nu^T = C_3\, \nu^{-\alpha} + C_4\, \nu^{-0.1} \quad . \qquad \text{(A.5)}$$

There is no simple way to solve simultaneously for C_3, C_4 and α even with three measurements at three different frequencies because the equations would not be independent of each other and they are not linear. If one could determine α independently, then at least two observations would suffice to solve for the non-thermal and thermal emission, because equation (A.5) would transform into a linear equation.

Since the value of α as observed in galaxies is between -0.7 and -1.2 (Gioia, Gregorini and Klein 1982), the predicted non-thermal flux at high frequencies (say 14.94 GHz) would be lower than the flux at low frequencies (say 1.49 GHz) and therefore any high flux value at 14.94 GHz would indicate a thermal origin as well. Although in principle two observations would suffice to derive an implicit equation involving the thermal emission and the spectral index α, a third observation at a higher frequency would be desirable in order to better estimate the thermal and non-thermal emissions. A basic derivation of the thermal emission at 14.94 GHz (2 cm) in terms of the observed fluxes at 1.49 and 4.86 GHz (20 and 6 cm) and the spectral index α would be as follows.

The total observed flux is the sum of non-thermal and thermal emissions,

$$S_{20}^T = S_{20}^{NTH} + S_{20}^{TH} \quad , \qquad \text{(A.6)}$$

$$S_6^T = S_6^{NTH} + S_6^{TH} \quad , \qquad \text{(A.7)}$$

$$S_2^T = S_2^{NTH} + S_2^{TH} \quad . \qquad \text{(A.8)}$$

The non-thermal emission at one frequency can be expressed in terms of the non-thermal emission at another frequency and the spectral index α as

$$S_{20}^{NTH} = S_6^{NTH}\, (\nu_{20}/\nu_6)^{-\alpha} \quad . \qquad \text{(A.9)}$$

Finally the thermal emission at one frequency can be expressed in terms of the thermal emission at another frequency as

$$S_{20}^{TH} = S_6^{TH}\, (\nu_{20}/\nu_6)^{-0.1} \quad , \qquad \text{(A.10)}$$

$$S_6^{TH} = S_2^{TH}\, (\nu_6/\nu_2)^{-0.1} \quad . \qquad \text{(A.11)}$$

The combination of (A.6) to (A.11) would then give

$$S_2^{TH} = \frac{S_{20}^T \left(\frac{\nu_2}{\nu_{20}}\right)^{-0.1} - S_6^T \left(\frac{\nu_{20}}{\nu_6}\right)^{-\alpha} \left(\frac{\nu_2}{\nu_{20}}\right)^{-0.1}}{\left[1 - \left(\frac{\nu_{20}}{\nu_6}\right)^{-\alpha} \left(\frac{\nu_6}{\nu_{20}}\right)^{-0.1}\right]} \quad . \qquad \text{(A.12)}$$

The advantage of this equation is that for any source the thermal emission at 2 cm is given in terms of the observed total fluxes at 20 and 6 cm, provided that the three observations are done with similar angular resolution; the disadvantage of this equation is that it is still a function of the spectral index α. One way to solve this problem would be to find a source that shows no thermal emission and obtain α. One then would assume that the α found would be characteristic of the non-thermal emission from the other source and when inserted in equation (A.12) one would finally obtain the thermal emission at 2 cm.

F. Combes and M. Gerin: DEMIRM, Observatoire de Meudon, 92195 Meudon, France.
R.-J. Dettmar: Radioastronomisches Institut der Universität Bonn, Auf dem Hügel 71, D-5300 Bonn 1, Germany.
J.A. García-Barreto: Instituto de Astronomía, UNAM, Apartado Postal 70-264, 04510 México, D.F., México.
B. Koribalski: Max-Planck-Institut für Radioastronomie, Auf dem Hügel 69, D-5300 Bonn 1, Germany.

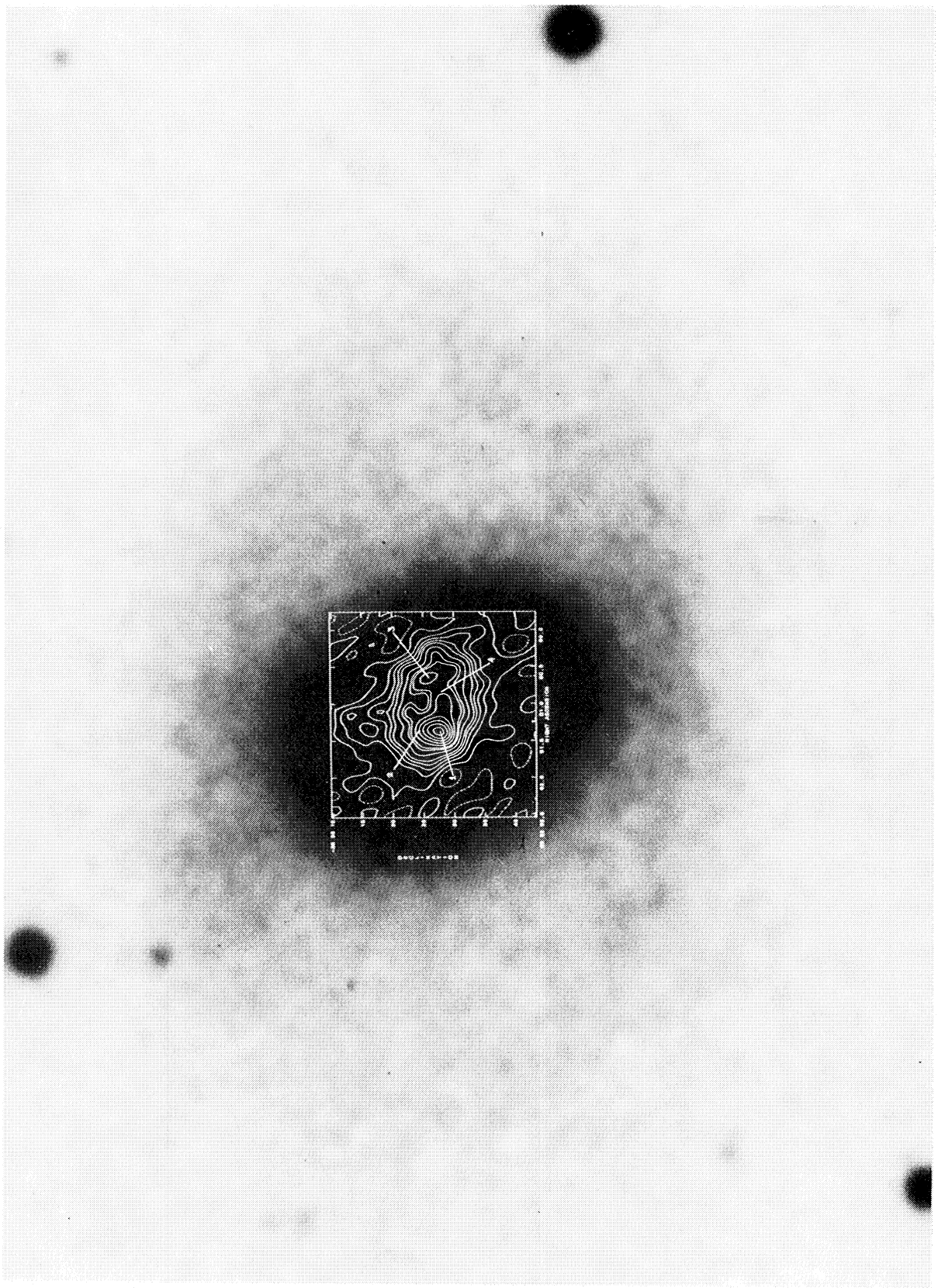

Fig. 5. Radio map of NGC 1326 at 20 cm superposed on a POSS O plate. The contour levels of the radio map are the same as in Figure 1. Relative alignment of the radio map and the optical picture is only accurate to ±3" in either direction.

J.A. GARCIA-BARRETO ET AL. (See page 197)

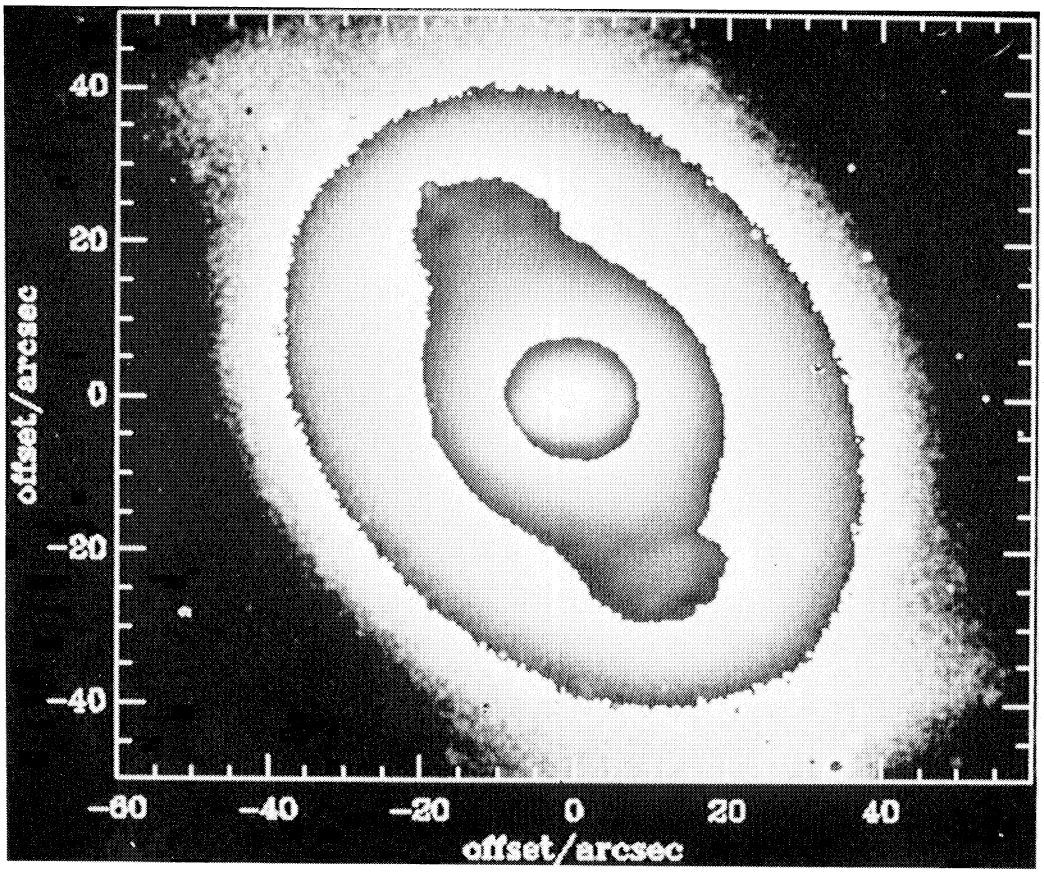

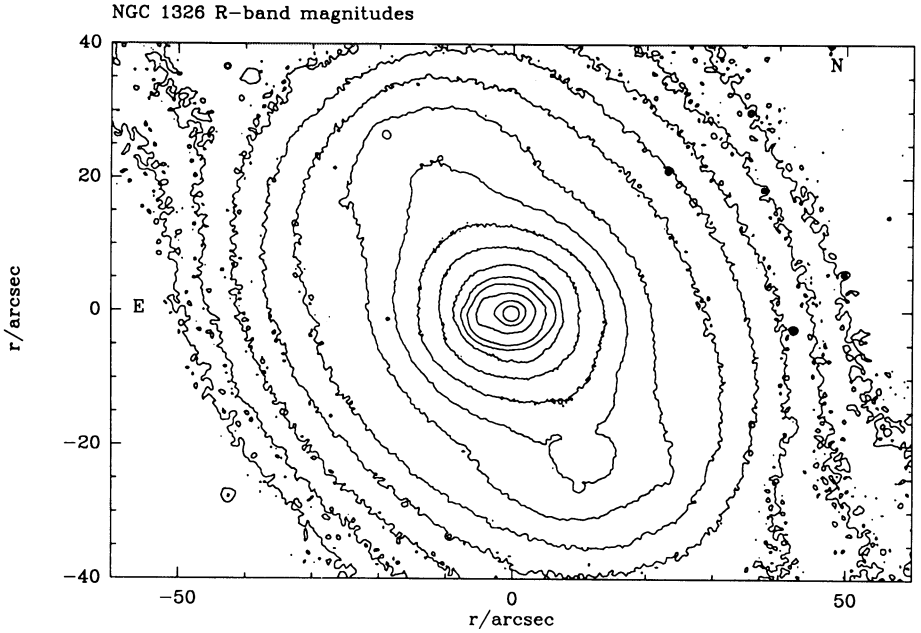

Fig. 6a. Grey scale R-band continuum of NGC 1326 taken at ESO 2.2-m telescope on La Silla (Chile). The bar structure is noticeable at PA $\sim 30°$. The field of view is 2.5'× 1.7'.

Fig. 6b. Contour R-band continuum image of NGC 1326. The lowest contour is $\mu_R \simeq 23$ mag arcsec^{-2}; the contour step is $\Delta\mu_R = 0.5$.